Model calculations of high-harmonic generation in molecular ions

R. Kopold and W. Becker*
Max-Born-Institut, Rudower Chaussee 6, 12489 Berlin, Germany

M. Kleber
Physik-Department T30, Technische Universität München, 85748 Garching, Germany

(Received 9 March 1998)

One electron bound by a three-dimensional two-center zero-range potential is embedded in an electric field with sinusoidal time dependence and arbitrary polarization and orientation with respect to the axis of the two-center potential. In the absence of the field, the model supports up to two bound states, which have a large transition dipole moment. Hence, the physical systems best described by the model are molecular ions such as H_2^+. Rates for high-harmonic emission are calculated analytically up to one final quadrature. In terms of the rescattering picture, harmonic emission can be attributed to two different mechanisms: electrons recombine either at the center they started from or at the other one. The latter case allows for three topologically different classes of orbits, which lead to different spectral ranges of harmonics. Two of them are similar to atomic (one-center) harmonic generation, but have different cutoff laws that are no longer proportional to the ponderomotive potential. In the third the electron moves directly from one center to the other. This leads to strong harmonic emission at comparatively low frequencies similar to emission from a two-level atom with the cutoff proportional to the field amplitude rather than the intensity. The molecular dipole phase in this case is almost independent of the field intensity and, at constant intensity, the phases of neighboring harmonics are locked. Different orientations of the two-center system with respect to the field with various polarization configurations are investigated. Most of the observed features lend themselves to interpretation in terms of the simple man's model. [S1050-2947(98)09111-2]

PACS number(s): 32.80.Rm

I. INTRODUCTION

If a nonlinear bound system is irradiated by an intense laser field it reradiates harmonics of the incident field. Depending on the incident intensity the spectrum may extend up to very high harmonics. In particular, there is an extended range of harmonics (the so-called plateau) that are radiated with comparable intensities. For the case where the bound system is atomic these phenomena have been intensively studied over the past decade, both experimentally and theoretically, and are now well understood; for reviews see Refs. [1,2]. The harmonics have already been employed as light sources for other experiments [3]. Ultimately, they may lead to novel sources of light with very unprecedented properties [4].

The investigation of multiphoton phenomena in molecules has been pioneered by the work of Fedorov *et al.* [5], which pointed out the significance of field-induced avoided crossings to molecules irradiated by intense laser fields and predicted the existence of light-induced states. With the advent of above-threshold ionization in atoms, interest picked up also in the interaction of intense lasers with molecules [6,7]. In particular, the work of Bucksbaum, Muller, and collaborators [8] reported the observation of a variety of field-induced effects in molecular systems, interpreted them in terms of field-dressed states, and coined terms such as bond softening and above-threshold dissociation. Owing to its structural simplicity, they concentrated on H_2^+, which became the object of a large number of experimental and theoretical investigations; for a review see Ref. [9]. Several intense-field molecular phenomena have been discovered in close contact between theory and experiment, such as population trapping and the relevance of internal tunneling ionization versus internal barrier suppression ionization. All of these mechanisms can be recovered in simulations based on solutions of the time-dependent Schrödinger equation.

Molecules as sources of high harmonics have been studied experimentally already several years ago and found to yield radiation patterns very similar to atoms [10]. Currently, clusters of atoms are being investigated [11]. They offer promising prospects as to raising the up to now disappointingly low conversion efficiency for harmonic generation.

Theoretical investigations of high-harmonic emission in molecular ions such as H_2^+ were first presented in Refs. [12, 13], which both drew attention to the relevance of charge-resonant states [14] to harmonic generation in these systems. A pair of charge-resonant states consists of an even-parity and an odd-parity state with a transition dipole moment that for large internuclear separation grows proportionally to this distance. They are characteristic of odd-charge molecular ions. These states strongly couple to an external field and produce harmonics efficiently. The corresponding harmonic generation is closely related to that calculated for the idealization of a quantum mechanical two-level system [15]. Ivanov and Corkum [12] concentrate on the two-level aspects inherent in the molecular ions while Zuo, Chelkowski,

*Also at Center for Advanced Studies, Department of Physics and Astronomy, University of New Mexico, Albuquerque, NM 87131.

and Bandrauk [13] solve the three-dimensional time-dependent Schrödinger equation with a two-center Coulomb potential in the Born-Oppenheimer approximation and recover both the two-level features and the aspects related to the common rescattering mechanism, which is responsible for harmonic generation in atoms. Recent work by these authors allows for self-consistently coupled nuclear motion [16].

The physical understanding of the process of high-harmonic generation has been boosted by the semiclassical three-step model or simple man's model [17,18], which is embedded into a fully quantum mechanical description [19–21]. In this class of models, the classical action of an electron in the laser field plays the dominant role while the atomic binding potential does little more than defining the binding energy and a source point (or region) where electrons are first injected into the laser field and later again disappear by recombination emitting their acquired energy through harmonic radiation. In terms of such modeling, a molecule or a cluster mainly differs from an atom by providing more than one center where the electron can appear on the scene or retire from it. This allows for a new feature: the electron promoted into the continuum may travel from one center to a different one in the process of harmonic emission. Investigating the implications of this mechanism provides the motivation of the present work.

As the simplest case we explore an electron bound by two zero-range potentials. With total ionization rates of the negative hydrogen molecular ion H_2^- in view, the two-center zero-range potential has already been investigated extensively in Ref. [22]. In the context of high-harmonic generation, it will turn out that the physical system most closely related to this model is the positive hydrogen molecular ion H_2^+.

The features that are specific for high-harmonic radiation by molecular ions have not been identified in experiments yet. They require internuclear separations of the order 5 to 10 Bohr radii in order to become significant. This realm becomes accessible in highly excited vibrational states or would be passed during Coulomb explosion. For realistic predictions of the harmonic emission to be expected in a given situation, the *collective* response of the sample must be evaluated [1,2] with the single-molecule response being the input. Even with current computing capabilities this is out of reach if the single-molecule input is calculated from the three-dimensional Schrödinger equation. A sufficiently compact yet realistic model is needed for the former. Judging from the comparison of our present results with three-dimensional Schrödinger simulations [13,16], the two-center zero-range potential can serve as such a model.

In Sec. II, we introduce the two-center zero-range potential and briefly review its properties and its relation to physical systems, in particular to homonuclear molecular ions. We then go on to calculate the S matrix for emission of a harmonic photon for arbitrary orientation of the molecular axis with respect to the plane of the elliptically polarized driving laser field. The ease with which three-dimensional effects can be treated is characteristic of zero-range potential models. As in the case of one zero-range potential the emission rates can be evaluated analytically up to one final quadrature, which is left for numerical computation. We give particular consideration to a circularly polarized driving field since, in contrast to the case of an atom, it does generate harmonics in a molecule. However, the mechanism is different from harmonic emission in an atom, viz., related to the two-level system and the existence of charge-resonant states, and consequently the typical plateau is absent. As in the atomic case, for linear polarization the simple man's model very nicely illuminates the origin of most of the features encountered in the harmonic spectrum. For the various spectral ranges of harmonic emission, we can identify electronic orbits that are responsible for them. In particular, the intense emission at comparably low frequencies is generated by electrons moving directly from one charge center to the other. In Sec. III, we present explicit results for harmonic spectra for typical configurations of the various parameters (internuclear separation, molecular binding energy, laser intensity, and polarization, and relative orientation of the molecular axis with respect to the laser). We investigate the intensity-dependent phase of the harmonic components of the field-induced molecular dipole element, which is known to be crucially important for the collective harmonic response [2]. Not surprisingly, this phase behaves much like in the case of an atom within the analog of the atomic plateau. However, it displays a strikingly different behavior within the low-energy two-level-related part of the spectrum: in this range it is virtually independent of the intensity. The consequences of this behavior for the propagation of the harmonic signal have not yet been explored. Also, in this regime neighboring harmonics are locked in phase with respect to each other. In a concluding section we emphasize some of our findings and discuss some deficiencies of the two-center zero-range potential. An Appendix discusses the question of which gauge to choose. As opposed to the one-center zero-range potential where the length gauge and the velocity gauge yield identical results for harmonic emission, the two-center zero-range potential mandates using the velocity gauge. Some reasons are discussed in the Appendix.

II. FORMAL FRAMEWORK

A. Two-center zero-range potential

An electron bound to the zero-range potential

$$V(\mathbf{r}) = \frac{2\pi\hbar^2}{\kappa m}\,\delta(\mathbf{r})\,\frac{\partial}{\partial r}r \tag{1}$$

provides the simplest model of an atom that still retains a full-fledged continuum. It has a single bound state with energy

$$E_0 = -\hbar^2\kappa^2/2m \tag{2}$$

and wave function

$$\phi_0(\mathbf{r},t) = \sqrt{\frac{\kappa}{2\pi}}\,\frac{e^{-\kappa r}}{r}\,e^{-iE_0 t/\hbar}. \tag{3}$$

The continuum wave functions are plane waves augmented by an s-wave term such that completeness including the bound state (3) is warranted. Since in the interaction of atoms and molecules with high-intensity laser fields the continuum is of crucial importance while the detailed structure

of the bound-state spectrum is not, the zero-range potential has yielded a good description of intense-field phenomena.

In order to model the behavior of one electron in the presence of a two-center binding potential we will consider a superposition of two zero-range potentials situated at positions $\mathbf{R}_1$ and $\mathbf{R}_2$

$$V(\mathbf{r})=\frac{2\pi\hbar^2}{m}\left(\frac{1}{\kappa_1}\delta(\mathbf{r}_1)\,\frac{\partial}{\partial r_1}r_1+\frac{1}{\kappa_2}\delta(\mathbf{r}_2)\,\frac{\partial}{\partial r_2}r_2\right), \quad (4)$$

where $\mathbf{r}_i=\mathbf{r}-\mathbf{R}_i$ and $\mathbf{R}=\mathbf{R}_1-\mathbf{R}_2$, $|\mathbf{R}|=R$. An exact solution of the corresponding Schrödinger equation can be found from an ansatz as a linear combination of atomic orbitals (3) with centers at $\mathbf{R}_1$ and $\mathbf{R}_2$,

$$\phi(\mathbf{r},t)=e^{-iE_0t/\hbar}\left(c_1\frac{e^{-\kappa r_1}}{r_1}+c_2\frac{e^{-\kappa r_2}}{r_2}\right) \quad (5)$$

with the binding energy (2) as given above. If inserted in the Schrödinger equation the ansatz (5) yields a linear homogeneous system for the coefficients c_1 and c_2,

$$\begin{pmatrix}\kappa_1-\kappa & e^{-\kappa R}/R\\ e^{-\kappa R}/R & \kappa_2-\kappa\end{pmatrix}\begin{pmatrix}c_1\\ c_2\end{pmatrix}=0. \quad (6)$$

The condition that its determinant vanish,

$$(\kappa_1-\kappa)(\kappa_2-\kappa)=\frac{e^{-2\kappa R}}{R^2}, \quad (7)$$

determines the binding energy (2) as well as the ratio

$$\frac{c_1}{c_2}=\frac{e^{-\kappa R}}{R(\kappa-\kappa_1)}=\frac{R(\kappa-\kappa_2)}{e^{-\kappa R}}. \quad (8)$$

Normalization of the wave function (5) completely fixes the coefficients c_1 and c_2 via

$$\frac{\kappa}{2\pi}=c_1^2+c_2^2+2c_1c_2e^{-\kappa R}. \quad (9)$$

The (positive) solutions κ of the determinant equation (7) fix the bound-state energy (2). They are easily discussed in graphical form. The result can be summarized as follows. If both κ_1 and κ_2 are positive there are two solutions if $\kappa_1\kappa_2R^2\geqslant 1$ and one solution otherwise. If both κ_1 and κ_2 are negative there is one solution if $\kappa_1\kappa_2R^2\leqslant 1$ and no solution otherwise. If κ_1 and κ_2 have opposite sign there is always exactly one solution. If $\kappa_1=\kappa_2$ there are two solutions if $\kappa_1R\geqslant 1$ (the one with the lower energy symmetric and the other one antisymmetric), one solution if $1>\kappa_1R\geqslant -1$ (symmetric), and no solution if $\kappa_1R<-1$.

In the limit where $R\to\infty$, the determinant equation (7) yields $\kappa=\kappa_1$ or $\kappa=\kappa_2$ and, consequently (for $\kappa_1\neq\kappa_2$), $c_2=0$ or $c_1=0$, respectively. That is, the limit of two separate centers is realized, the electron stays near one center and does not notice the other. In contrast, the limit where the two centers coincide is tricky. One may expect that in this limit the wave function (5) reduces to the one-center wave function (3) with κ given by $1/\kappa=1/\kappa_1+1/\kappa_2$, but this is not so. Rather, the determinant condition (7) demands that $\kappa\to\infty$ in the limit where $R\to 0$ so that the binding energy would become infinite. A comparable situation occurs in the linear-combination-of-atomic-orbitals description of H_2^+ with Coulomb potentials; see, e.g., Ref. [24]. For $R\to 0$, the LCAO approximation of the wave function fails to approach the ground-state wave function of He^+. Here we will not be concerned with this limit and refer to Refs. [23,22] for a discussion.

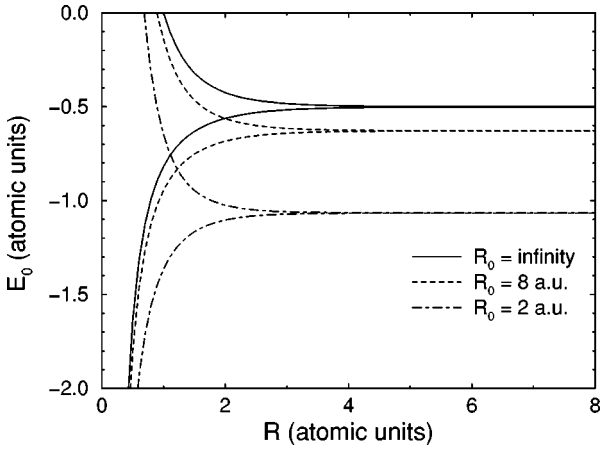

FIG. 1. Bound-state energies of the two-center zero-range potential with two equivalent centers as a function of the separation R between the two centers. The parameter $\kappa_1=\kappa_2$ of the model potential (4) has been adjusted so as to yield the known binding energy of H_2^+ at some internuclear separation R_0. Examples are exhibited for three different values of R_0 as indicated. In each case, the excited bound state ceases to be bound for $R<1/\kappa_1$ as discussed below Eq. (9).

The two-center zero-range potential (4) has three parameters, the distance R between the two centers, and the respective strengths related to the parameters κ_1 and κ_2. There is, in principle, a multitude of ways of how to adjust these parameters to the properties of a particular physical system. *A priori*, it is not even clear whether the two-center zero-range potential is better suited to model, for example, H_2, H_2^+, or H_2^- (after all, the one-center zero-range potential is known to make a very good model of H^-). Let us concentrate on the case of two equivalent centers. For $\kappa_1=\kappa_2\geqslant 1/R$ there are two bound states. It is easy to see that they become degenerate for $R\to\infty$; cf. Fig. 1. In this limit the solutions (5) have the form

$$\phi(\mathbf{r},t)_{s,a}=\phi_1\pm\phi_2, \quad (10)$$

with identical values of κ. The transition dipole moment simply becomes

$$\mathbf{d}_{as}\equiv\langle\phi_a|\mathbf{r}|\phi_s\rangle=\mathbf{R}/2. \quad (11)$$

This situation is characteristic of charge resonant states [14,12,13] such as they exist in H_2^+, but not in H_2 or H_2^-. Hence, whenever we will make reference to a particular physical system it will be H_2^+. The exact value of the transition dipole moment calculated with the help of the wave functions (5) for finite R is

$$\mathbf{d}_{as}=2\pi c^a c^s\mathbf{R}\left(\frac{1}{s}+\frac{1+s}{s^2\Delta^2}e^{-s}(\Delta\,\cosh\Delta-\sinh\Delta)\right), \quad (12)$$

where $s=R(\kappa_s+\kappa_a)/2$ and $\Delta=R(\kappa_s-\kappa_a)/2$ and κ_s and κ_a are the wave numbers of the symmetric and the antisymmetric bound state, respectively. For simplicity, two equivalent centers were assumed. The expression shows that for increasing R the limit (11) is attained very quickly.

In order to adjust the parameters to the case of H_2^+ for a specified distance R_0 between the two protons, we solve Eq. (7) for κ and adjust $\kappa_1=\kappa_2$ such that the lower one of the two eigenenergies (2) agrees with the $(1s\sigma_g)$ ground-state energy of H_2^+ at the respective distance R_0. The corresponding ground-state energies have been calculated by accurate solution of the one-particle Schrödinger equation and are available in the literature [25]. If κ_1 is fixed as just described the bound-state energies of the two-center zero-range potential are determined for all R. Simultaneously, the energy of the $2p\sigma_u$ excited bound state is fixed by the model (if it exists, that is, if $\kappa_1 R_0 \geqslant 1$). Figure 1 shows three examples where $\kappa_1=\kappa_2$ has been adjusted to the binding energy of H_2^+ at three different distances, $R_0=2$ a.u., 8 a.u., and ∞ corresponding to two separate protons. If in the spirit of the Born-Oppenheimer approximation the appropriate Coulomb repulsion e^2/R is added one obtains the nuclear energy surfaces produced by the model potential. No matter what we choose for R_0 the ground-state potential surface has little in common with the actual $1s\sigma_g$ energy surface of H_2^+. In particular, it is not bonding. Hence, if we actually attempt to model field-induced processes in H_2^+ as a function of the internuclear distance, as we do in Fig. 8 below, we enforce the correct behavior by redetermining $\kappa_1=\kappa_2$ for each distance R that we consider.

The model of H_2^+ outlined in the preceding paragraph may come across as a rough caricature of this molecular ion. However, we do not intend to model H_2^+ per se, but rather H_2^+ *generating harmonics owing to the presence of an intense field*. Like a good caricature, it is intended to highlight the features of interest at the expense of obscuring others.

B. *S*-matrix element of harmonic emission

We decompose the total electromagnetic field into a classical part $\mathbf{A}_L(t)$ that describes the laser field and a quantized part $\mathbf{A}_q$ that is related to the mode of a high harmonic emitted by irradiating a bound system by the intense laser field $\mathbf{A}_L$. For reasons to be discussed in the Appendix we use the radiation gauge. The total Hamiltonian of the laser-matter system reads

$$H_{\text{total}}=H-\frac{e}{mc}\left(\mathbf{p}-\frac{e}{c}\mathbf{A}_L\right)\cdot\mathbf{A}_q+\frac{e^2}{2mc^2}\mathbf{A}_q^2, \tag{13}$$

with

$$H=\frac{\mathbf{p}^2}{2m}+V(\mathbf{r})-\frac{e}{mc}\mathbf{A}_L\cdot\left(\mathbf{p}-\frac{e}{2c}\mathbf{A}_L\right) \tag{14}$$

the Hamiltonian of the atom interacting with the *classical* laser field $\mathbf{A}_L(t)$ while the terms that incorporate the *quantized* field $\mathbf{A}_q$ cause emission and absorption of high-harmonic photons. The term proportional to $\mathbf{A}_q^2$ does not contribute to one-photon emission or absorption. Now, the *S*-matrix element for the emission of one photon with polarization $\boldsymbol{\epsilon}$ and frequency Ω is

$$M(\boldsymbol{\epsilon},\Omega)=ie\sqrt{\frac{2\pi}{\Omega\hbar V}}\int_{-\infty}^{\infty}dt e^{i\Omega t}\boldsymbol{\epsilon}^*\cdot\mathbf{v}(t), \tag{15}$$

where

$$\begin{aligned}\mathbf{v}(t)&=\langle\psi_f^{(+)}(t)|\dot{\mathbf{r}}|\psi_i^{(-)}(t)\rangle\\&=\frac{1}{m}\langle\psi_f^{(+)}(t)|\mathbf{p}-(e/c)\mathbf{A}_L(t)|\psi_i^{(-)}(t)\rangle.\end{aligned} \tag{16}$$

The wave functions $\psi_{i,f}^{(\pm)}(t)$ satisfy boundary conditions such that they agree with the initial and final bound state $\phi_{i,f}(\mathbf{r},t)$ in the absence of the laser field, respectively, in the limit of early and late times,

$$\lim_{t\to-\infty}\psi_i^{(-)}(\mathbf{r},t)=\phi_i(\mathbf{r},t)\quad\text{and}\quad\lim_{t\to\infty}\psi_f^{(+)}(\mathbf{r},t)=\phi_f(\mathbf{r},t). \tag{17}$$

For reasons that will be discussed below we will, with the help of an integration by parts, express the *S*-matrix element (15) in dipole form. We employ the equation of motion

$$i\hbar\dot{\mathbf{r}}=\frac{i\hbar}{m}\left(\mathbf{p}-\frac{e}{c}\mathbf{A}_L\right)=[\mathbf{r},H], \tag{18}$$

where H is the full Hamiltonian so that $H\langle\psi_{i,f}|=i\hbar\partial_t\langle\psi_{i,f}|$ and insert it in the velocity form (15). This yields

$$M(\boldsymbol{\epsilon},\Omega)=ie\boldsymbol{\epsilon}^*\cdot\sqrt{\frac{2\pi}{\Omega\hbar V}}\int_{-\infty}^{\infty}dt e^{i\Omega t}\partial_t\langle\psi_f^{(+)}(t)|\mathbf{r}|\psi_i^{(-)}(t)\rangle \tag{19}$$

$$=e\boldsymbol{\epsilon}^*\cdot\sqrt{\frac{2\pi\Omega}{\hbar V}}\int_{-\infty}^{\infty}dt e^{i\Omega t}\langle\psi_f^{(+)}(t)|\mathbf{r}|\psi_i^{(-)}(t)\rangle. \tag{20}$$

The boundary terms occurring in the partial integration that led from Eq. (19) to Eq. (20) do not contribute to a transition *rate* and have been omitted.

The *S*-matrix element (20) is still in the radiation gauge even though it contains the dipole matrix element. At this point we approximate the wave functions $|\psi_{i,f}^{\pm}(t)\rangle$ in the spirit of the Keldysh approximation. We follow a procedure introduced earlier [21]. In the matrix element

$$\begin{aligned}\mathbf{R}(t)&=\langle\psi_f^{(+)}(t)|\mathbf{r}|\psi_i^{(-)}(t)\rangle\\&=\lim_{t'\to\infty,t''\to-\infty}\langle\phi_f(t')|U(t',t)\mathbf{r}U(t,t'')|\phi_i(t'')\rangle,\end{aligned} \tag{21}$$

we employ the (Dyson-) integral equation for the exact time evolution operator $U(t,t')$ in the radiation gauge. Then introducing the crucial approximation we replace the exact time evolution operator U by the Volkov time evolution op-

erator $U^{(V_R)}$ and perform several integrations by parts [21]. We end up with the compact form

$$\mathbf{R}(t)\approx -\frac{1}{\hbar^2}\int_{-\infty}^{t}dt''\int_{t}^{\infty}dt' \times\langle\phi_f(t')|VU^{(V_R)}(t',t)\mathbf{r}U^{(V_R)}(t,t'')V|\phi_i(t'')\rangle. \tag{22}$$

This expression simplifies considerably if one realizes [26] that

$$\langle\mathbf{r}'|U^{(V_R)}(t',t)\mathbf{r}U^{(V_R)}(t,t'')|\mathbf{r}''\rangle = \mathbf{r}_{\rm class}(t;\mathbf{r}'t',\mathbf{r}''t'')\langle\mathbf{r}'|U^{(V_R)}(t',t'')|\mathbf{r}''\rangle. \tag{23}$$

Here,

$$\mathbf{r}_{\rm class}(t;\mathbf{r}'t',\mathbf{r}''t'')\equiv\frac{1}{t'-t''}\left\{(t-t'')\left(\mathbf{r}'-\frac{e}{cm}\int_{t'}^{t}d\lambda\mathbf{A}(\lambda)\right) -(t-t')\left(\mathbf{r}''-\frac{e}{cm}\int_{t''}^{t}d\lambda\mathbf{A}(\lambda)\right)\right\} \tag{24}$$

denotes the trajectory as a function of time t of a classical particle from the initial position $\mathbf{r}''$ at time t'' to the final position $\mathbf{r}'$ at time t' in the presence of a field given by the vector potential $\mathbf{A}(t)$. With the help of Eqs. (21)–(24), the matrix element (20) assumes the form

$$M(\boldsymbol{\epsilon},\Omega)=-\frac{e\boldsymbol{\epsilon}^*}{\hbar^2}\sqrt{\frac{2\pi\Omega}{\hbar V}}\int dte^{i\Omega t}\int d^3r'd^3r''\int_{t}^{\infty}dt' \times\int_{-\infty}^{t}dt''\phi_f^*(\mathbf{r}',t')V(\mathbf{r}')U^{(V_R)}(\mathbf{r}',t';\mathbf{r}'',t'') \times\mathbf{r}_{\rm class}(t;\mathbf{r}',t';\mathbf{r}'',t'')V(\mathbf{r}'')\phi_i(\mathbf{r}'',t''). \tag{25}$$

This will be the starting point for the explicit calculations below.

Had we not performed the integration by parts in Eq. (19) then we would have arrived at a form like Eq. (25) but with $\mathbf{v}_{\rm class}=\dot{\mathbf{r}}_{\rm class}$ in place of $\mathbf{r}_{\rm class}$. It turns out that the end points of the classical trajectory (at $t=t''$ and $t=t'$) make particularly important contributions to the matrix element. At these end points, however, $\mathbf{v}_{\rm class}$ is discontinuous: it jumps from an ensemble average of zero, corresponding to a bound state, to a finite value. Moreover, near these end points the approximation of ignoring the binding potential is least justified. On the other hand, after the integration by parts, the matrix element contains $\mathbf{r}_{\rm class}$ whose end points

$$\mathbf{r}_{\rm class}(t;\mathbf{r}'t',\mathbf{r}''t'')=\begin{cases}\mathbf{r}' & \text{for}\quad t=t'\\ \mathbf{r}'' & \text{for}\quad t=t''\end{cases} \tag{26}$$

are well defined and independent of any approximation made. This is why we performed the integration by parts that led from Eq. (19) to (20).

C. Explicit results for the *S*-matrix element

The computation of the S-matrix element can be carried out analytically all the way down to one final integration, which is left for numerical evaluation. The calculation is fairly straightforward though lengthy and the procedure is similar to the case of just one center [20] where extensive details are presented. We will therefore just give an outline and essentially be content with writing down the final result. Details for the present case can be found in Ref. [30].

From the structure of the wave function (5) it is clear that the matrix element (25) has the form

$$M(\boldsymbol{\epsilon},\Omega)=\sum_{j,k=1}^{2}c_j^fc_k^iM_{jk}(\boldsymbol{\epsilon},\Omega), \tag{27}$$

where $c_n^{i,f}$ is the coefficient in the wave function (5) of the initial and final state, respectively, that determines the probability of the electron being near center n. The decomposition (27) allows for the identification of the contribution where the electron departs from the center k in the initial state and returns to the center j in the final state. For the evaluation we assume a monochromatic elliptically polarized laser field specified by the vector potential

$$\mathbf{A}_L(t)=A_L[\mathbf{e}_x\cos(\omega t)+\mathbf{e}_y\xi\sin(\omega t)]. \tag{28}$$

The lengthy calculation yields

$$M_{jk}(\boldsymbol{\epsilon},\Omega)=-8\pi^2e\sqrt{\frac{i\Omega}{m\omega V}}\boldsymbol{\epsilon}^*\cdot\sum_{n=1}^{\infty}\delta(\Omega-n\omega)\int_0^{\infty}\frac{d\tau}{n\tau^{3/2}}e^{i[(E_0/\hbar\omega)\tau+iS_0(\mathbf{R}_j-\mathbf{R}_k,\tau)]}\left\{\left[-i\cos\left(\frac{n\tau}{2}\right)\frac{\mathbf{R}_j-\mathbf{R}_k}{2} +\sin\left(\frac{n\tau}{2}\right)\left(i\frac{\mathbf{R}_j-\mathbf{R}_k}{n\tau}+\frac{\mathbf{R}_j+\mathbf{R}_k}{2}\right)\right]\Sigma_n(s_1(\tau),s_{jk}(\tau),\vartheta_{jk}) +\frac{eA_L}{2\omega mc}[(i\mathbf{e}_x+\xi\mathbf{e}_y)g^+(n,\tau)\Sigma_{n+1}(s_1(\tau),s_{jk}(\tau),\vartheta_{jk}) +(i\mathbf{e}_x-\xi\mathbf{e}_y)g^-(n,\tau)\Sigma_{n-1}(s_1(\tau),s_{jk}(\tau),\vartheta_{jk})]\right\}. \tag{29}$$

The integration variable τ/ω can be interpreted as the time that the electron having started from the kth center spends in the continuum until it reaches the jth center and recombines. The abbreviations used here originate from the Volkov propagator, which has the form

$$U^{(V_R)}(\mathbf{r}',t';\mathbf{r}'',t'')=\left(\frac{m}{2\pi i\hbar(t'-t'')}\right)^{3/2}\exp\frac{i}{\hbar}S(\mathbf{r}',t';\mathbf{r}'',t'') \tag{30}$$

with the action

$$\frac{1}{\hbar}S(\mathbf{r}',t';\mathbf{r}'',t'')=s_0[\mathbf{r}'-\mathbf{r}'',\omega(t'-t'')] + \cos\,\omega(t'+t'')s_1[\omega(t'-t'')] \tag{31}$$

$$+\cos\frac{\omega}{2}(t'+t'')s_2[\mathbf{r}',\mathbf{r}'',\omega(t'-t'')] -\sin\frac{\omega}{2}(t'+t'')s_3[\mathbf{r}',\mathbf{r}'',\omega(t'-t'')]. \tag{32}$$

Its ingredients are the functions

$$s_0(\mathbf{r},\tau)=\frac{m\omega\mathbf{r}^2}{2\tau\hbar}-\eta\tau\left(1-\frac{4\sin^2\,\tau/2}{\tau^2}\right), \tag{33}$$

$$s_1(\tau)=\eta\zeta\left(-\sin\,\tau+\frac{4\sin^2\,\tau/2}{\tau}\right), \tag{34}$$

where

$$\eta=\frac{U_p}{\hbar\omega}=\frac{e^2A_L^2(1+\xi^2)}{4m\hbar\omega c^2},\quad \zeta=\frac{1-\xi^2}{1+\xi^2} \tag{35}$$

are commonly used parameters related to the intensity and polarization, respectively, of the laser field (28). The two functions s_0 and s_1 have the same form in any gauge while

$$s_2(\mathbf{r}',\mathbf{r}'',\tau)=\frac{eA_L}{\hbar c}(x'-x'')\frac{2}{\tau}\sin\frac{\tau}{2}, \tag{36}$$

$$s_3(\mathbf{r}',\mathbf{r}'',\tau)=-\frac{eA_L}{\hbar c}\xi(y'-y'')\frac{2}{\tau}\sin\frac{\tau}{2} \tag{37}$$

are gauge specific. The form given here is for the radiation gauge, which is used in this paper. The functions s_{jk} and ϑ_{jk} that enter the matrix element M_{jk} [Eq. (29)] have to be determined from

$$s_2(\mathbf{R}_j,\mathbf{R}_k,\tau)=s_{jk}(\tau)\sin(\vartheta_{jk}),$$
$$s_3(\mathbf{R}_j,\mathbf{R}_k,\tau)=s_{jk}(\tau)\cos(\vartheta_{jk}). \tag{38}$$

They all depend on $\mathbf{R}_j$ and $\mathbf{R}_k$. Generalized Bessel functions are used as defined by

$$\Sigma_\nu(a,b,c)=\sum_{l=-\infty}^{\infty}i^lJ_l(a)J_{\nu-2l}(b)e^{i(\nu-2l)c}. \tag{39}$$

Finally, we have defined the functions

$$g^{\pm}(n,\tau)=-\frac{1}{n\pm1}\sin(n\pm1)\frac{\tau}{2}+\frac{2}{n\tau}\sin\frac{n\tau}{2}\sin\frac{\tau}{2}. \tag{40}$$

We now restrict ourselves to the case where the initial and the final states are identical so that $c^f=c^i$ and the molecule is in the end, after the laser pulses has passed through, in the same state as before. We place the origin half-way between the two centers so that $\mathbf{R}_1=-\mathbf{R}_2=\mathbf{R}/2$. The final form of the matrix element (29) is different for odd and even harmonics. In the first case the matrix element reads

$$M(\boldsymbol{\epsilon},\Omega)=8\pi^2ie\sqrt{\frac{i\omega}{m\Omega V}}\,\boldsymbol{\epsilon}^*\cdot\sum_{n=1}^{\infty}\delta(\Omega-(2n-1)\omega)\int_0^\infty\frac{d\tau}{\tau^{3/2}}e^{i\varepsilon_0\tau}\Big[(c_1^2+c_2^2)e^{is_0(0,\tau)}i^n\{(\mathbf{e}_x-i\xi\mathbf{e}_y)g^+(2n-1,\tau)J_n(s_1(\tau))$$
$$-i(\mathbf{e}_x+i\xi\mathbf{e}_y)g^-(2n-1,\tau)J_{n-1}(s_1(\tau))\}+c_1c_2e^{is_0(\mathbf{R},\tau)}\Big\{\mathbf{R}\Big(\frac{2}{(2n-1)\tau}\sin(2n-1)\frac{\tau}{2}$$
$$-\cos(2n-1)\frac{\tau}{2}\Big)\Sigma_{2n-1}(s_1(\tau),s_{12}(\tau),\vartheta_{12})+\alpha(\mathbf{e}_x-i\xi\mathbf{e}_y)g^+(2n-1,\tau)\Sigma_{2n}(s_1(\tau),s_{12}(\tau),\vartheta_{12})$$
$$+\alpha(\mathbf{e}_x+i\xi\mathbf{e}_y)g^-(2n-1,\tau)\Sigma_{2n-2}(s_1(\tau),s_{12}(\tau),\vartheta_{12})\Big\}\Big]. \tag{41}$$

A much simpler expression is obtained for the even harmonics

$$M(\boldsymbol{\epsilon},\Omega)=4\pi^2(c_1^2-c_2^2)e\sqrt{\frac{i\omega}{m\Omega V}}\,\boldsymbol{\epsilon}^*\cdot\mathbf{R}\sum_{n=1}^{\infty}\delta(\Omega-2n\omega) \times\int_0^\infty\frac{d\tau e^{i\varepsilon_0\tau}}{\tau^{3/2}}e^{is_0(0,\tau)}\sin(n\tau)i^nJ_n(s_1(\tau)). \tag{42}$$

However, for reasons detailed in the Appendix this expression may not yield a reliable estimate of the emission of even harmonics. The quantity

$$\alpha=\frac{eA_L}{m\omega c} \tag{43}$$

denotes the excursion amplitude (for linear polarization) of

an electron oscillating in the continuum subject to the laser field (28).

It is instructive to inspect the dependence of these S-matrix elements on the internuclear separation $\mathbf{R}$. The coefficients c_1 and c_2 of the wave function (5) specify the probability that the electron is found at the first or the second center. The matrix element (41) for the emission of odd harmonics consists of two terms, one being proportional to $c_1^2+c_2^2$ and the other to c_1c_2. The first term contains those contributions to harmonic emission where the electron returns to the center from which it started. In contrast, in the second it moves from one center to the other. We will refer to these two terms as the ''return term'' and the ''exchange term,'' respectively. The return term is independent of the distance between the two centers. It is the sum of one contribution from each center and, correspondingly, its form agrees with the S matrix for harmonic emission by just one zero-range atom [20]. Also, this term goes to zero as it should in the limit of circular polarization where $s_1(\tau)$ vanishes. In contrast, the exchange term does depend on $\mathbf{R}$ through the functions $s_0(\tau)$, $s_{12}(\tau)$, and ϑ_{12}. The overall factor $\exp[is_0(\mathbf{R},\tau)]$ ensures that it does not grow forever as $\mathbf{R}$ increases. For circular polarization, the exchange term survives in simplified form: the generalized Bessel function (39) reduces to an ordinary one. The resulting expression is discussed below.

For two equivalent centers ($\kappa_1=\kappa_2$) parity invariance holds and, as a consequence, even harmonics cannot be emitted. Indeed, the S-matrix element (42) vanishes in this case owing to $|c_1|=|c_2|$. Parity also mandates that the S-matrix element (41) for the odd harmonics does not depend on the sign of $\mathbf{R}$, which indeed it does not.

The expression (42), which we calculated for even harmonics is problematic. It does vanish for equivalent centers (where $|c_1|=|c_2|$) as it should, but it does so for circular polarization, too, even for nonequivalent centers. However, there is no general conservation law that prohibits emission of even harmonics for two inequivalent centers irradiated by a circularly polarized field. Moreover, the matrix element is just proportional to $\mathbf{R}$ with no damping for increasing distance. In order to get a reliable expression for the emission of even harmonics, the approximation that led to Eq. (25) must be improved. Some dressing of the ground state is required. This can be achieved by further iteration of the Dyson equation for the exact time-evolution operator $U(t,t')$, but will not be attempted in this paper.

D. Circular polarization of the driving field

There is a pronounced difference between harmonic generation by an atom and by a molecule: the latter allows, in general, for the emission of harmonics of a *circularly* polarized driving field. The origin of this difference can be understood by attempting to construct the nonlinear susceptibility tensor $\chi^{(n)}_{i,i_1,i_2,\ldots,i_n}$ of the atom on the one hand or the molecule on the other. The polarization of the atom or molecule (viz., its time-dependent dipole moment) is

$$P_i(t)=\sum_{n=1}^{\infty}\sum_{i_1,i_2,\ldots,i_n}\int_0^{\infty}d\tau_1\cdots d\tau_n \times\chi^{(n)}_{i,i_1,\ldots,i_n}(\tau_1,\ldots,\tau_n)E_{i_1}(t-\tau_1)\cdots E_{i_n}(t-\tau_n). \tag{44}$$

All of the properties of the respective atom or molecule (in the absence of the field) are contained in the tensors $\chi^{(n)}$. For a monochromatic driving field,

$$\mathbf{E}\sim\mathbf{e}\,\exp(-i\omega t)+\mathbf{e}^*\,\exp(i\omega t), \tag{45}$$

a term with fixed value of n generates harmonics up to the nth order.

First, let us recall the case of an atom. If the binding potential as well as the relevant initial and final state obey spherical symmetry, the susceptibility tensor has to be constructed out of Kronecker tensors δ_{ij} as these are the only ones available in view of the spatial isotropy of the atom [27]. This only allows for the construction of $\chi^{(n)}$ with an even number of indices, that is $\chi^{(3)}$, $\chi^{(5)}$, etc. Moreover, when calculating the polarization (44) of the atom one contracts the susceptibility tensor with the driving field (45). In order to generate the nth harmonic we need at least n terms $\mathbf{e}\exp(-i\omega t)$ from the field (45). For circular polarization, the polarization vector $\mathbf{e}=(\mathbf{e}_x\pm i\mathbf{e}_y)/\sqrt{2}$ satisfies $\mathbf{e}\cdot\mathbf{e}=0$ while $\mathbf{e}^*\cdot\mathbf{e}=1$. Since the susceptibility tensor consists of products of Kronecker tensors, the polarization vectors $\mathbf{e}$ will have to be contracted with themselves. As a consequence, all harmonic components of the polarization $\mathbf{P}$ are identically zero.

For a two-center binding potential the situation is completely different. The spatial isotropy is violated by the existence of the vector $\mathbf{R}$, which specifies the orientation of the molecule. This vector can be employed in the construction of the susceptibility tensor so that the aforementioned contractions of the polarization vector with itself can be avoided. Hence, arbitrary harmonic components result that are non-

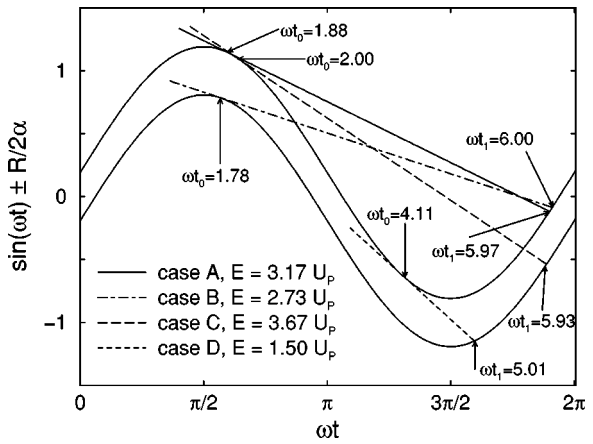

FIG. 2. Graphical determination of the return (or recombination) time t_1 according to Eq. (49). Four qualitatively different scenarios are depicted. Case A is analogous to the single-atom situation. In case B and C the electron starts at one center and recombines at the other bypassing along its way either the center it started from (case C) or the other one [at which it is going to recombine (case B)]. In case D the electron starts at one center and moves directly to the other. The parameters used in the figure are those from Fig. 4 for $R=12$ a.u., which shows explicit calculations. The trajectories depicted correspond to maximal classical recombination energies which along with the times t_0 and t_1 were calculated from Eqs. (52)–(54). Notice that the assignments in terms of multiples of U_p are specific for the parameters used (with the exception of $3.17U_p$, which holds universally).

zero provided only that $\mathbf{e}\cdot\mathbf{R}\neq 0$. Also, owing to the existence of the vector $\mathbf{R}$, we can now construct tensors $\chi^{(n)}$ with even n. For two equivalent centers, however, the sign of $\mathbf{R}$ must not play any role, so χ's with even n vanish as before.

These considerations are borne out by the explicit matrix element. For circular polarization ($\xi=1$, say) we have $s_1(\tau)\equiv 0$, and the general S-matrix element (41) for the odd harmonics reduces to ($\Omega>\omega$)

$$M(\boldsymbol{\epsilon},\Omega)=8\pi^2 ie\sqrt{\frac{i\omega}{m\Omega V}}\,\boldsymbol{\epsilon}^*\cdot\sum_{n=2}^{\infty}\delta(\Omega-(2n-1)\omega)\int_0^\infty\frac{d\tau}{\tau^{3/2}}e^{i\varepsilon_0\tau}$$
$$\times c_1c_2e^{is_0(2\mathbf{R},\tau)}e^{i(2n-1)\vartheta_{12}}\Bigg[\mathbf{R}\left(\frac{2}{(2n-1)\tau}\sin(2n-1)\frac{\tau}{2}-\cos(2n-1)\frac{\tau}{2}\right)J_{2n-1}(s_{12}(\tau))$$
$$+\alpha(\mathbf{e}_x-i\mathbf{e}_y)g^+(2n-1,\tau)J_{2n}(s_{12}(\tau))e^{i\vartheta_{12}}+\alpha(\mathbf{e}_x+i\mathbf{e}_y)g^-(2n-1,\tau)J_{2n-2}(s_{12}(\tau))e^{-i\vartheta_{12}}\Bigg]. \qquad (46)$$

As it should be, it is exclusively due to the exchange term. If the orientation of the molecule is perpendicular to the plane of the polarization so that $(\mathbf{e}_x\pm i\mathbf{e}_y)\cdot\mathbf{R}=0$, then $s_{12}(\tau)\equiv 0$ [cf. the definition of this function in Eqs. (36)–(38)], and there is no harmonic emission.

The polarization of the emitted harmonics can be calculated from the matrix element (46). It is, in general, elliptic and there are no simple rules regarding the orientation of the plane of polarization. If, however, the molecular axis lies in the plane of polarization of the driving field then the harmonics are polarized in this plane as well.

III. THE SIMPLE MAN'S MODEL

The simple classical model where an electron starts its orbit at the center of the binding potential with zero velocity, thereafter follows a classical trajectory in the presence of merely the laser, and depending on its time of departure returns to its site of release to recombine into the atomic ground state emitting its acquired kinetic energy plus the binding energy in the form of one harmonic photon—this model has contributed to the understanding of high-harmonic generation more than anything else [17,18]. It is also embedded in realistic quantum models [19,20]. The extension to two-center binding potentials is straightforward and has been discussed before [28]. We briefly summarize the relevant formulas.

The trajectory verbally depicted above is

$$\mathbf{r}(t)=\mathbf{r}_0+\frac{e}{mc}\left((t-t_0)\mathbf{A}(t_0)-\int_{t_0}^{t}d\tau\mathbf{A}(\tau)\right) \qquad (47)$$

with t_0 the departure time at position $\mathbf{r}_0$ and $\mathbf{A}(t)$ the vector potential of the laser field, in this paper specified by Eq. (28). We are interested in those times t_1, viz. the recombination times, when the electron either returns to its starting point or arrives at the other center of the binding potential. These times are defined by

$$\mathbf{r}(t_1)-\mathbf{r}_0=\mathbf{R}_1-\mathbf{R}_2 \quad \text{or} \quad 0. \qquad (48)$$

For general elliptic polarization, this vector equation only has solutions for particular pairs of t_1 and t_0. For linear polarization, there is just one equation to be solved and there are solutions $t_1\equiv t_1(t_0)$ for whole regions of t_0. A common procedure for elliptic polarization (provided the ellipticity ξ is not too large) is to solve only the component of the return condition (48) that corresponds to the large component of the field and to ignore the other. The physical reasoning behind this procedure is the rapid spreading of the wave packet associated with such a classical trajectory, which implies that it does not matter whether the electron returns exactly to a particular point or just into some vicinity; see, e.g., [29].

For our elliptically polarized field (28), the x component is the large component. So the applicable return condition is

$$\sin\,\omega t_1=\sin\,\omega t_0+\omega(t_1-t_0)\cos\,\omega t_0+\begin{cases}0\\ \pm R_x/\alpha,\end{cases} \qquad (49)$$

where R_x denotes the projection of the internuclear separation $\mathbf{R}$ on the direction of the large component of the field and the excursion amplitude α was defined in Eq. (43). The solutions of the return condition (49) are easily discussed graphically. Figure 2 depicts the two functions $\sin\omega t\pm R_x/2\alpha$. For given t_0, the return condition (49) asks one to draw the tangent at time t_0 to either one of these two curves and then to intersect it with the same curve (for an electron that returns to the center it started from) or with the other one (for an electron that starts at one center and recombines at the other) in order to determine the recombination time t_1. These tangents define electron trajectories, and we will use these two terms interchangeably. Several relevant examples are explicitly shown and labeled. Case A is the same as for one atom: the electron returns to the center it started from. The tangent drawn is for $t_0=1.88$, which yields $t_1=5.97$. This is the situation that corresponds to the maximal return energy of $3.17U_p$. Of course, the same tangent can be drawn with respect to the other (lower) curve (not shown). This latter tangent would bypass the other center on the way forth as well as back. However, within the simple man's model as well as in the expression (25) the electron is not affected by the presence of the binding potential except at the instant when it recombines. Figure 2 depicts two other tangents, which are closely related to A. Tangent B starts from one center and recombines at the other, and so does tangent C.

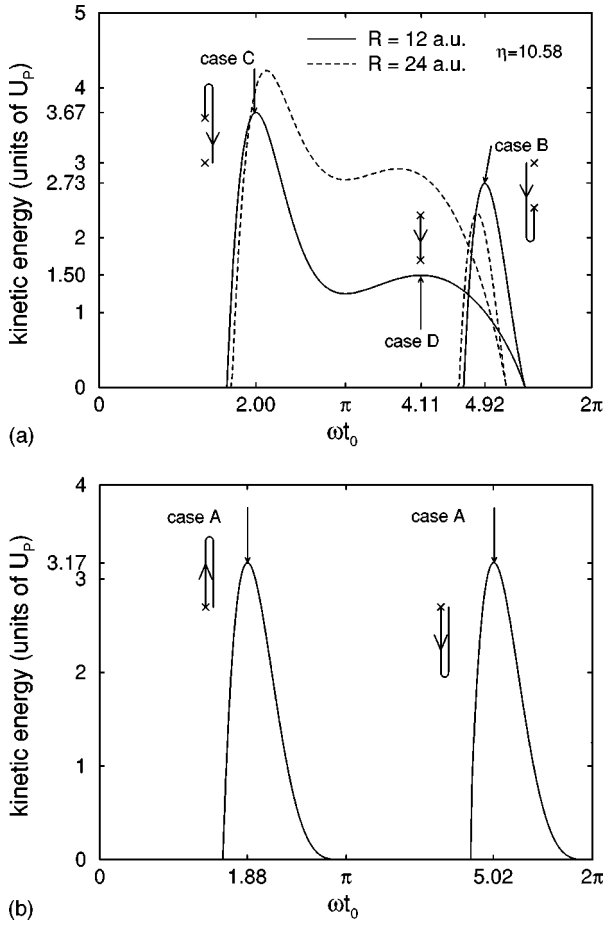

FIG. 3. Recombination energies as a function of the start time t_0 for a single atom (b) and for the two-center zero-range potential (a) with the parameters from Figs. 2 and 4 for $R=12$ a.u. and 24 a.u. For each of the three scenarios B, C, and D a typical trajectory is sketched.

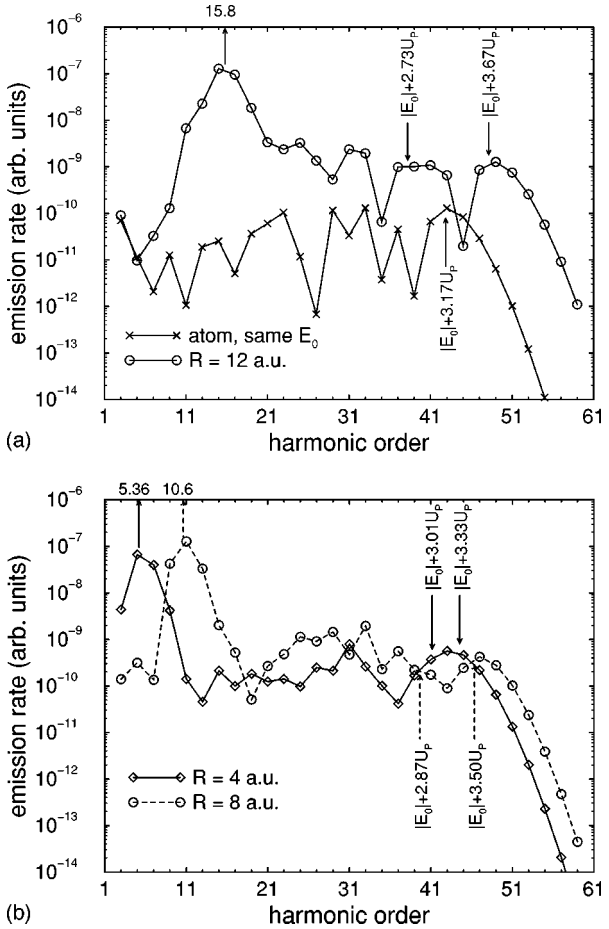

FIG. 4. Comparison between harmonic spectra for a two-center system for various separations R and the spectrum of a single atom. The two-center system is aligned with the linearly polarized driving field. The parameters are $\omega=0.043$ a.u., $\eta=U_p/(\hbar\omega)=10.58$, and the binding energy is $|E_0|=0.4$ a.u. The distance between the two centers is $R=0$ and $R=12$ a.u. (a), and $R=4$ a.u. and $R=8$ a.u. (b). In each case the maximal classical recombination energies given in the right half of the figure are calculated from the simple man's Eqs. (52)–(54). For each separation, the lower energy corresponds to scenario B and the higher one to scenario C. The energy assignments in the upper left indicate the maximum harmonic number of the low-energy hump as calculated from Eq. (51).

Both B and C are drawn for those start times t_0 that yield maximal kinetic energies at the time t_1 of recombination as determined from Eqs. (52) and (53) below. The tangents B and C are topologically different. The trajectory B starts moving towards the center at which it will recombine while C starts moving away from it. As a consequence, the two associated maximal kinetic energies are different. Typically, the recombination energy corresponding to B exceeds that of C. Finally, there is a completely new solution labeled D, unprecedented from the case of one atom. Here the electron moves directly from one center to the other. Again, the tangent depicted is the one that yields a maximal recombination energy. However, in contrast to the other cases A, B, and C, in case D there is (provided the distance R is not too large) a large interval of start times t_0 all of which lead to comparable recombination times t_1 and energies. This is illustrated in Fig. 3: for example, for $R=12$ a.u., start times within the quite extended interval $2.8\lesssim\omega t_0\lesssim 4.4$ all result in comparable recombination energies between $1.25U_p$ and $1.5U_p$, and the associated interval of return times t_1 is much narrower than the interval of start times t_0.

When it returns the electron has gained the kinetic energy

$$E_{\mathrm{kin,ret}}=\frac{e^2}{2mc^2}[\mathbf{A}(t_1)-\mathbf{A}(t_0)]^2. \tag{50}$$

For a linearly polarized monochromatic field, obviously, $E_{\mathrm{kin,ret}}\leqslant 8U_p$. This upper limit is achieved when the departure time and the return time correspond to opposite maxima of the vector potential. For the field (28), with linear polarization, this happens for $t_0=0$ and $\omega t_1=(2n+1)\pi$, and the return condition (49) implies that the distance between the two centers must be

$$R=\alpha\pi(2n+1)=\frac{e\pi E_L}{m\omega^2}(2n+1). \tag{51}$$

For fields strong enough to generate substantial harmonic emission, this is a distance very large on the atomic scale.

Figure 3 displays the recombination energy as a function of the start time. The parameters are the same as in Figs. 2 and 4, internuclear separations are $R=12$ a.u. as well as 24 a.u. and for comparison the single-atom results are also depicted. For the latter, start times within the first half period of

the field yield precisely the same return energies as those in the second half period. For the two-center case, this is not so and the first half and the second half period lead to scenarios C and B, respectively. In between, there is a sizable range of start times t_0 such that the return energies are just below $1.5U_p$ (case D). Extrapolating the tendency from $R=12$ to 24 a.u. one can infer that for ever increasing R the two maxima of case C and D will finally merge to yield, for the distance (51), the absolute maximum of $8U_p$.

A relative maximum of the return (or recombination) energy (50) can be determined by equating to zero its derivative with respect to the start time t_0 taking into account that the return time t_1 is a function of t_0 via Eq. (49) [20]. This yields a trigonometric equation for the travel time $\rho=\omega(t_1-t_0)/2$, viz.,

$$(\sin\rho-\rho\cos\rho)^2-(\rho\sin\rho)^2 = \pm\frac{R}{2\alpha}\{(\sin\rho-\rho\cos\rho)^2+(\rho\sin\rho)^2\}^{1/2}, \tag{52}$$

whose solution allows for the determination of the start time through

$$\chi=\frac{\omega}{2}(t_1+t_0)=\arctan\frac{\rho\sin\rho}{\sin\rho-\rho\cos\rho}. \tag{53}$$

Finally, the corresponding return energies (50) can be obtained from

$$E_{\mathrm{kin,ret}}=8U_p\sin^2\rho\sin^2\chi. \tag{54}$$

In the derivation of Eqs. (52) and (53) $t_0\neq 0$ was assumed.

The tangents A to D depicted in Fig. 2 are the solutions of Eqs. (52) and (53). For $R=0$ all of this reduces, of course, to the customary situation for one atom yielding $3.17U_p$ for the maximal return energy, etc. It is important to realize that for $R=0$ Eqs. (52) and (53) do not contain any parameter at all. Hence the solutions ωt_0 and ωt_1 are independent of the laser intensity, and the return energy (54) is just proportional to U_p. This is no longer true for $R\neq 0$ where the laser intensity enters Eq. (52) for the travel time through the parameter α.

IV. RESULTS

All of the explicit results to be discussed in this section are calculated from the matrix element (41) for odd harmonics in the velocity gauge. We will restrict ourselves entirely to the case of equivalent centers such that $c_1=c_2$. Moreover, we will only consider emission processes where the atom occupies the same state (the ground state) before and after the passage of the laser pulse. Under these conditions, only odd harmonics of the driving field are radiated. For the interpretation we will often refer to the simple man's model discussed in the previous section.

A. Emission rates of the harmonics

In all cases the quantity that we will plot is the rate of emission per time and solid angle element of a photon with frequency Ω integrated over a small frequency interval around the center frequency. The polarization $\boldsymbol{\epsilon}$ is chosen so that the emission rate becomes maximal, that is, parallel to the direction defined by the S-matrix element (41). Since we employ the dipole approximation for the emitted photon as well as for the driving field, the emission rate obeys a dipole pattern.

Figure 4 compares harmonic emission by a single atom and by a two-center configuration, which is lined up with the linearly polarized laser field. Spectra are displayed for various distances between the two centers and the binding energy is kept constant. Comparing the one-atom spectrum with the two-center spectra one notices two conspicuous differences. First, harmonic production within the plateau is more efficient for two centers. Second, there is a low-energy part of the spectrum that is dramatically enhanced in the case of two centers. It forms a hump such that the energy of its top harmonic is proportional to the distance between the two centers. Here and below we will refer to this feature as the ''low-energy hump.'' As for the first observation, a very rough explanation of the general enhancement of the plateau is provided by the existence of two pathways for the electron to recombine: with the center it started from as well as with the other. As for the second, the hump corresponds to case D of Fig. 2 where the electron moves from one center to the other within a time interval that is short compared with the period of the field. Moreover, this happens around the time where the field is near its maximum. Therefore, we may approximate the electron's energy gain by

$$E_{\mathrm{kin,ret}}=eE_LR_x. \tag{55}$$

This yields energies very close to the values given in Fig. 4, which are determined from Eqs. (52)–(54). It is remarkable that the maximum of the hump is reproduced just by the energy (55) without the additional binding energy $|E_0|$, unlike the standard maximal energy of the plateau, viz., the cutoff energy $|E_0|+3.17U_p$. Figure 2 also suggests an explanation of why the hump is above the altitude of the plateau by several orders of magnitude. First, as mentioned above, the travel time is comparatively short so that the associated wave packet does not spread very much. Second, there is a quite large interval of start times t_0 all of which lead to comparable recombination times t_1 and energies $E_{\mathrm{kin,ret}}$. Hence, a time-frequency (or wavelet) analysis [32,33] should identify a very sharply defined temporal structure of the group of harmonics within the hump exhibiting two spikes within one optical period corresponding to the two recombination times t_1.

It is well known that a driven two-level atom exhibits a harmonic response also characterized by a kind of plateau and a cutoff whose position equals the recombination energy (55) [12,15,31]. Indeed, the symmetric and the antisymmetric solutions (3) of the two-center zero-range potential form a realization of a quantum mechanical two-level system. In the limit of large distance their wave functions approach the form (10), and their large transition dipole moment (11) dominates the interaction with the laser field. Hence, the two-center zero-range potential combines the harmonic spectrum of a two-level atom with the manifestations of the simple man's model in the continuum.

Yet another prediction of the simple man's model mate-

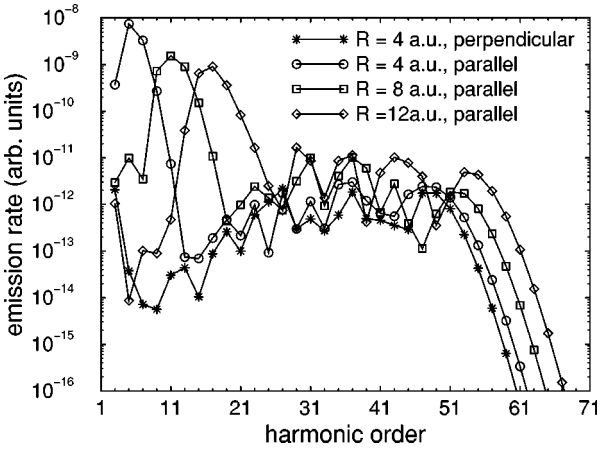

FIG. 5. Comparison of harmonic spectra for a two-center system oriented parallel (for various distances between the two centers) and perpendicular to a linearly polarized driving field. The parameters are $\omega=0.043$ a.u., $\eta=10.5$, and $|E_0|=0.566$ a.u.

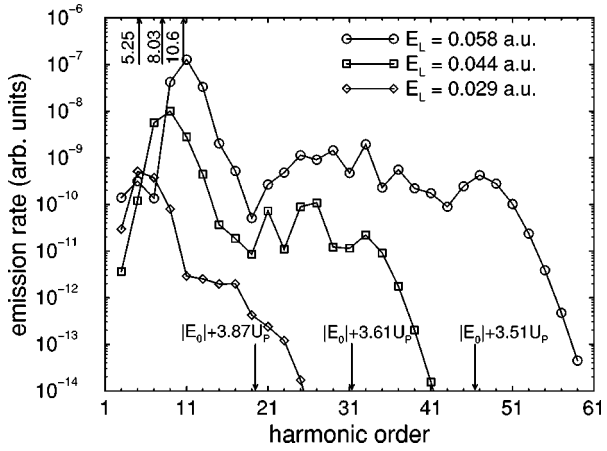

FIG. 6. Harmonic spectra for a two-center system with $R=8$ a.u. aligned with a linearly polarized driving field for various intensities, corresponding to $E_L=0.058$, 0.044, and 0.029 a.u. The other parameters are $\omega=0.043$ a.u. and $|E_0|=0.4$ a.u. For each case, the highest classical cutoff (scenario C) is given as well as the maximum of the low-energy hump expressed as a harmonic number.

rializes in the exact calculation of Fig. 4: this is the different energies corresponding to the solutions labeled B and C in Fig. 2. Both are generated by the electron moving from one center to the other, though not along the most direct route D, but rather following two topologically different trajectories as explained above. The separation in energy is clearly visible for the larger internuclear distances $R=8$ a.u. and 12 a.u. Interestingly, these two maxima completely mask the standard cutoff at $3.17U_p$ as the distance grows larger.

Figure 5 compares harmonic spectra where the two-center system is aligned with the field with a case where it is perpendicular. For a separation of 4 a.u., within the plateau the two spectra show little difference between parallel and perpendicular alignment. However, for the low harmonics the difference is huge. For parallel alignment, the aforementioned hump dominates the spectrum. For perpendicular orientation, it is absent and the spectrum is very close to the case of the single atom.

Figure 6 gives an example of how the spectra depend on the intensity of the driving field. In each case the cutoff positions calculated from the simple man's model, that is from Eqs. (52)–(54), are indicated. They reproduce the cutoffs of the exact calculations very well. The figure also displays how the center of the hump scales with the field: It follows precisely the simple prediction (55). Finally, Fig. 7 illustrates the scaling of the spectra with the binding energy $|E_0|$. As known from the case of one atom, the scaling of the plateau is dramatic. For the comparatively small distance of 4 a.u. chosen for this figure, the cutoff of the plateau displays perfect agreement with the standard estimate of $|E_0|+3.17U_p$. In impressive contrast, the position of the hump is completely independent of the binding energy. Also, its height is less dependent on the binding energy than the height of the plateau. Both Figs. 6 and 7 are for parallel alignment.

While Figs. 4–7 illustrate general properties of harmonic production by an academic two-center zero-range potential, in Fig. 8 we attempt to simulate H_2^+ as closely as possible within this model. The internuclear distances are moderate, from 2 to 8 a.u., and for each separation R the binding energy E_0 $[=E_0(R)]$ was adjusted to the respective binding energy of H_2^+ taken from Ref. [25] as described in Sec. II A. All of the features observed above are recovered, including the hump for low energies and its absence for perpendicular alignment, and the splitting of the spectrum just before the cutoff for large separation. The plateau is strongly enhanced for the larger separations. However, this is predominantly a consequence of the lower binding energy for larger separation, cf. Fig. 7.

The dependence of the harmonic spectrum on the orientation of the two-center system with respect to the field is investigated in Fig. 9. When the axis turns from parallel to the field to perpendicular the hump gradually disappears. For parallel alignment, the parameter $R_x/\alpha=1.73$ is quite large. Hence, the different trajectories B and C (in the nomenclature introduced in connection with Fig. 2) clearly manifest themselves in the two cutoffs at about $N=13$ and $N=19$. The parameters have been chosen so that for parallel alignment the results can be directly compared with calculations of Ref. [16], which numerically solve the time-dependent

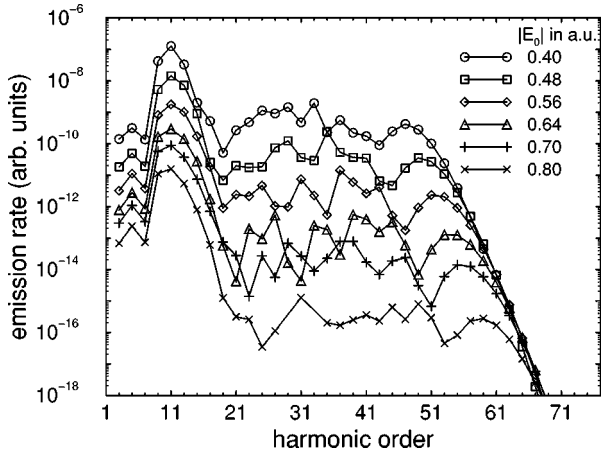

FIG. 7. Harmonic spectra for a two-center system with $R=8$ a.u. aligned parallel to a linearly polarized driving field with $\eta=10.58$ and $\omega=0.043$ for various binding energies.

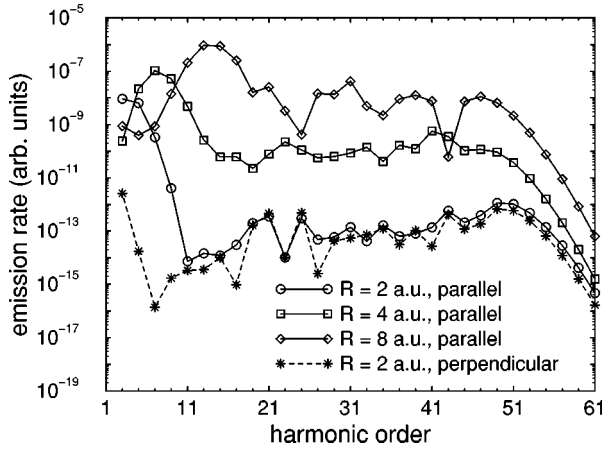

FIG. 8. Harmonic spectra for a two-center system modeled to simulate H_2^+ for various distances between the two protons, $R=2$ a.u. ($|E_0|=1.103$ a.u.), $R=4$ a.u. ($|E_0|=0.796$ a.u.), and $R=8$ a.u. ($|E_0|=0.628$ a.u.). In all cases the molecule is lined up with the linearly polarized driving field with $\omega=0.076$ a.u. and $\eta=10.58$. For $R=2$ a.u. the spectrum for perpendicular orientation is also given.

Schrödinger equation, both with and without the Born-Oppenheimer approximation. Qualitatively and semiquantitatively, many features are closely related, in particular the position and magnitude of the low-energy hump. The most noticeable discrepancy is in the dropoff beyond the plateau, which is much faster in our results. Figure 10 elucidates the dependence of the harmonic spectrum on the ellipticity of the driving field in the case where the molecular axis is aligned with the large component of the driving field. Here, with increasing ellipticity, the hump survives though it becomes less pronounced while the plateau disappears. For a circularly polarized driving field, a two-center system does emit harmonics. However, the common return-of-the-electron-to-the-core mechanism is no longer applicable and, as a consequence, there is no plateau. The harmonics that are emitted are due to the mechanism of trajectory *D* in Fig. 2: twice during one optical cycle the circularly polarized field is parallel to the axis and capable of driving the electron directly from one center to the other. Finally, Fig. 11 illustrates the transition from linear to circular polarization for the case where the axis of the two-center system is perpendicular to the small component of the driving field. Here, when the polarization is close to linear, the hump is absent.

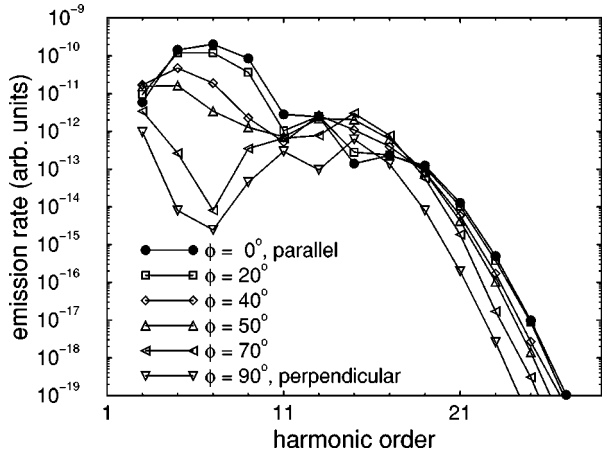

FIG. 9. Harmonic spectra for a two-center system with $R=8$ a.u. changing its orientation from parallel to perpendicular to the linearly polarized driving field. The remaining parameters are $\omega=0.076$ a.u., $\eta=1.62$, and $|E_0|=0.65$ a.u. For parallel alignment, the parameters agree with those of Fig. 10 of Ref. [16].

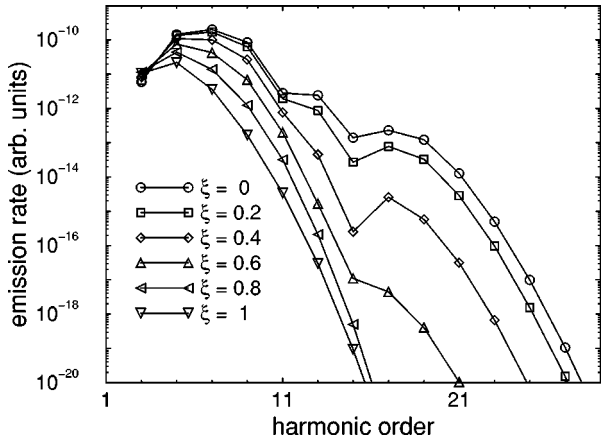

FIG. 10. Harmonic spectra for a two-center system with $R=8$ a.u. oriented parallel to the large component of an elliptically polarized driving field when the ellipticity changes from linear to circular. The remaining parameters are as in Fig. 9.

B. Phases of the harmonics

The *S*-matrix elements governing harmonic emission are complex. Thus far we have concentrated on their magnitudes, which determine the probability of emission of a harmonic photon. The physical significance of their phases is not immediately obvious. We recall, however, that for harmonic emission owing to its characteristically low efficiency the *S*-matrix element and the expectation value of the dipole matrix element are practically identical [21]. The physical relevance of the latter is very well established [34,35]: it provides crucial input for the behavior of the collective response. With this motivation in mind, we will investigate the phases of the *S*-matrix elements for the two-center system.

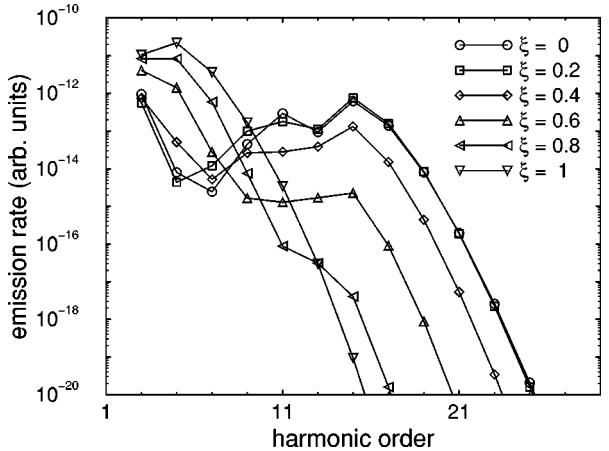

FIG. 11. Same as Fig. 9, but the two-center system is oriented parallel to the small component of the elliptically polarized driving field.

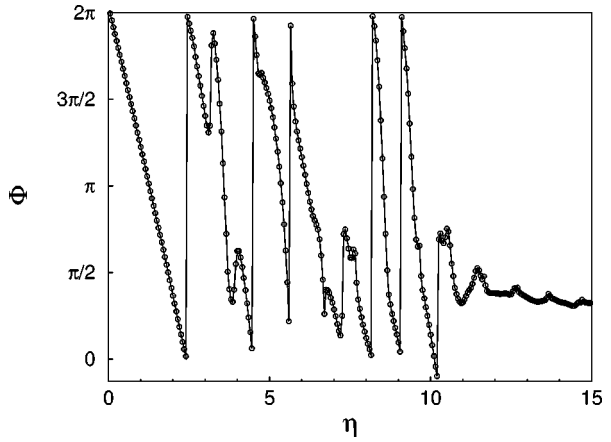

FIG. 12. Phase of the S-matrix element for emission of the 21st harmonic for a two-center system with $R=12$ a.u., aligned parallel to the linearly polarized driving field, as a function of its intensity specified by $\eta=U_p/(\hbar\omega)$. The remaining parameters, $|E_0|=0.4$ a.u. and $\omega=0.043$ a.u. are those of Fig. 4. The two simpleman cutoffs as calculated from Eqs. (52)–(54) are $\eta=2.7$ (scenario C) and $\eta=4.54$ (scenario B).

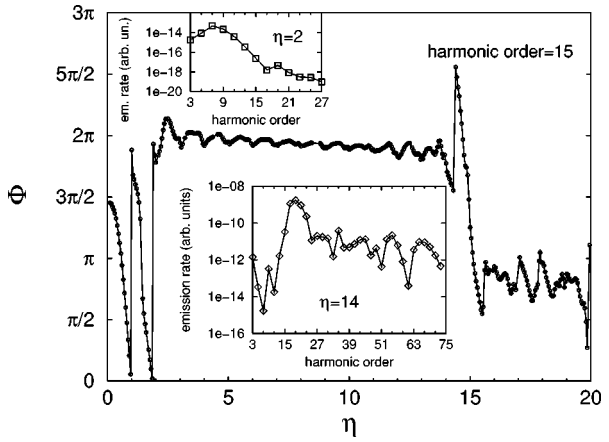

FIG. 13. Same as Fig. 12, but for the 15th harmonic and $|E_0|=0.6$ a.u. The two insets show harmonic emission rates under the same conditions for $\eta=2$ and for $\eta=14$ in order to present evidence that the 15th harmonic is part of the low-energy hump for $2\lesssim\eta\lesssim14$.

A typical result is given in Fig. 12, which displays the phase of the 21st harmonic for the parameters of Fig. 4 and $R=12$ a.u. as a function of the driving intensity expressed by the dimensionless parameter $\eta=U_p/\hbar\omega$. Up to $\eta\lesssim10$ the behavior is completely familiar from the one-atom case, see e.g., Refs. [35,36]: below $\eta\lesssim3$ the 21st harmonic is beyond the cutoff of the plateau and, consequently, the phase drops proportionally to about 3η. At $\eta=3.69$, the 21st harmonic enters the plateau, and the phase starts exhibiting the associated typical erratic behavior. At the same time, its *average* rate of decrease approximately doubles. However, at $\eta\approx10$ something unexpected happens: the phase becomes largely independent of the intensity. Inspection of Fig. 4 reveals that at about this intensity the 21st harmonic enters the low-energy hump from above, that is, from the region of high harmonics. It appears that harmonics within the hump are characterized by a phase that is almost independent of the intensity. This is confirmed by Fig. 13. The two insets demonstrate that in this case the 15th harmonic is part of the low-energy hump for intensities in the range specified by $2\lesssim\eta\lesssim15$ and, indeed, it is throughout precisely this range that the phase is virtually independent of the intensity. For $\eta\lesssim2$, the 15th harmonic briefly belongs to the plateau until for $\eta\lesssim0.5$ it has moved beyond the cutoff. On the other hand, on the high-intensity side of the hump, the phase shows behavior that is reminiscent of the low harmonics in the one-atom case, those below the plateau which are well described by lowest-order perturbation theory. Again, the intensity dependence of the phase is not very pronounced. (The harmonics that make up the hump are, however, not accessible to lowest-order perturbation theory.) For $\eta\gtrsim20$ (not shown), the 15th harmonic is definitely part of the plateau, and its phase behaves accordingly.

The fact that the phase is almost independent of the intensity for harmonics within the hump can be understood by inspection of the action (31) in the time-evolution operator (30), which is the essential input in the matrix element (25). The harmonics in the hump are due to trajectories of type D as defined in Figs. 2 and 3. They unfold near the maximum of the driving field. Therefore, in order to scrutinize their properties, we may approximate the action by the limit of a constant driving field letting $\omega\to0$, $A_L\to\infty$ while $\omega A_L=cE_L=\text{const}$. Then

$$\begin{aligned}S(\mathbf{r}'t',\mathbf{r}''t'')&=\frac{m(\mathbf{r}'-\mathbf{r}'')^2}{2(t'-t'')}-\frac{1}{2}eE_L(x'-x'')(t'+t'')\\&\quad-\frac{(eE_L)^2}{24m}(t'-t'')^3\\&=\frac{m\omega R^2}{2\tau}\pm\sqrt{\eta m\hbar\omega}R_x\omega(t'+t'')-\frac{1}{6}\hbar\eta\tau^3,\end{aligned}\tag{56}$$

where $\tau\equiv\omega(t'-t'')$. In the second line of the preceding equation, the action is specialized to exchange terms and rewritten in dimensionless quantities. The first term on the right-hand side is independent of the intensity, and the second only depends on the sum $t'+t''$. Let us envision a stationary-phase evaluation of the integrals in the matrix element (25). For the harmonics within the hump, the integral with respect to the time difference $t'-t''$ (which corresponds to the travel time) will be stationary for a travel time of t_1-t_0 corresponding to the trajectory of type D. For the conditions of Fig. 2 we have $\tau=\omega(t_1-t_0)\approx0.9$. The intensity dependence of the phase is then determined by the last term on the right-hand side of the action (56), which is equal to -0.12η in this case. This must be compared with -3.3η in the case of a single atom for the harmonics beyond the cutoff [20]. Hence, for harmonics within the low-energy hump the phase depends only very weakly on the driving intensity. The preceding argument followed Refs. [34,2].

Figure 14 compares the phase for parallel and perpendicular alignment. Remarkably, the phase in the one-atom case (here that of the 15th harmonic) is virtually identical to the phase in case of the two-center system oriented perpendicularly to the field even though in the latter exchange terms make substantial contributions. In contrast, the phase for par-

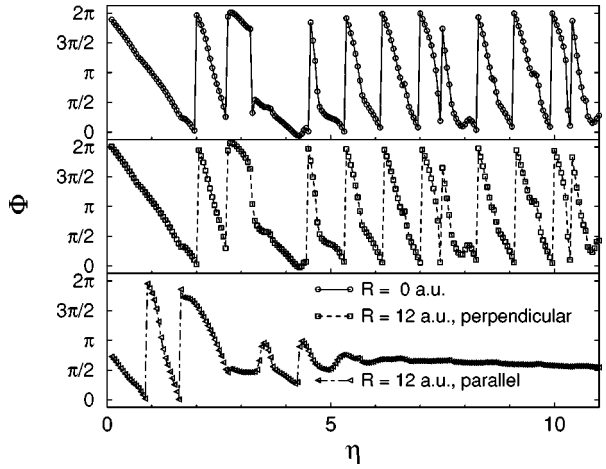

FIG. 14. Comparison of the phase of the S-matrix element for emission of the 15th harmonic by one atom (top), a two-center system with $R=12$ a.u. oriented perpendicularly to the field (middle), and the same oriented parallel to the field (bottom). The parameters are the same as in Figs. 12 and 4.

allel orientation shows evidence of the higher cutoff of the plateau (which is due to scenario C mentioned above) and becomes approximately constant when the 15th harmonic, at $\eta \approx 4$, enters the hump from below.

Finally, Fig. 15 points out that the harmonics within the hump are to some degree phase locked. (Harmonic emission rates for the same parameters are shown in Fig. 4.) For fixed intensity, the phases of adjacent harmonics are compared by plotting their differences $\phi_N - \phi_{N-2}$ as a function of N. First, as may have been expected, the well-known phase locking of the one-atom harmonics beyond the cutoff is recovered in the present two-center case. Also, as expected, it starts somewhat later at the higher cutoff corresponding to scenario C. This is clearly visible for the largest internuclear distance ($R=12$ a.u.) covered by this figure. In this case one may also observe a very brief interval of phase locking that starts at the lower cutoff corresponding to scenario B, but has no opportunity fully to develop since soon afterwards the higher cutoff begins to dominate with its own associated

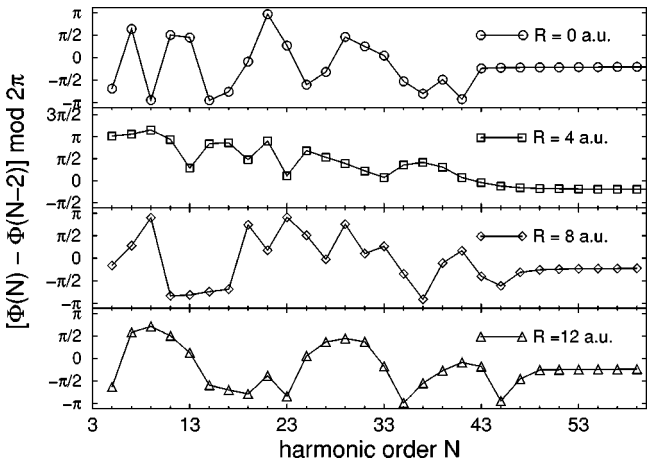

FIG. 15. Phase differences $\phi_N - \phi_{N-2}$ between adjacent harmonics as a function of the harmonic number N for $R=0$, 4, 8, and 12 a.u., respectively, from top to bottom. The parameters are those of Figs. 12 and 4.

phase locking. However, the novel feature of this figure is the phase locking of the harmonics within the hump. It is not as rigid as in the cutoff, but quite noticeable. It is most conspicuous for $R=8$ a.u.

For $R=4$ a.u. within the major part of the plateau the harmonic phases are not exactly but quite closely locked. This corresponds to the intensities (cf. Fig. 4 within the plateau which is for $R=4$ a.u. much less rugged than for the single atom. Apparently, two centers at a moderate distance that is much smaller than the width of the returning electronic wave packet tend to smooth the S-matrix element, both its magnitude and its phase, as a function of both driving intensity and harmonic number.

V. CONCLUSIONS

We have extended the zero-range potential model to one electron in a two-center zero-range potential in order to model, in particular, harmonic generation by molecular ions. Such a system combines the characteristic traits of harmonic generation in atoms (notably the extended plateau with a well-defined cutoff proportional to the ponderomotive potential) with those typical of a two-level system (a hump in place of a plateau with a cutoff proportional to the field amplitude). The two-level related features disappear when the orientation of the molecular axis changes from parallel to the laser field to perpendicular. In the latter case high-harmonic generation is very much atomlike. In a similar vein, if the two-center system is irradiated by a laser field with circular polarization the harmonic spectrum is essentially that of a two-level system. (The atom, after all, in a circularly polarized field produces no harmonics at all.) In contrast to an idealized quantum mechanical two-level system whose two-dimensional Hilbert space cannot be represented in ordinary space, here the two-level features manifest themselves in a very intuitive geometrical way: the electron moves from one center to the other. The simple man's model, which identifies particular electronic orbits in the presence of the laser field as responsible for particular spectral regions of harmonics, remains (for linear polarization) a very convenient tool with high predictive power.

The phases of the dipole components in the spectral region corresponding to two-level emission are strikingly different from the phases within the ordinary atomlike plateau. Their intensity dependence is very weak whereas in the plateau the phase changes by about 2π when the ponderomotive potential of the field changes by the energy $\hbar\omega$ of one photon. This will have a marked impact on the collective harmonic response of an ensemble of stretched molecular ions. Closely related is the fact that the phases of adjacent harmonics within the same spectral region are locked with respect to each other. The explicit calculations presented in this paper proceed sufficiently fast so that they can be used as the molecular input for the simulation of the collective response of an ensemble.

From the experimental point of view, it is crucial whether or not the orientation of the molecular ions with respect to the field can be controlled. There is a lot of accumulated evidence [8,9,37,38] that for laser pulses down to a pulse length of 100 fs molecules do become aligned with a linearly polarized field, either due to some dynamical mechanism

generated by the laser-molecule interaction [39,40] or, possibly, already by the way the molecular beam is prepared. (In exceptional cases, though, it has been predicted that the molecule orients itself perpendicularly to the field [40].) With a pump-probe experiment, then, molecules can be subjected to pulses with arbitrary polarization. Indeed, a high-intensity pump-probe experiment has been carried out recently where the probe field was polarized perpendicularly to the molecular axis [41].

The extension of the presently discussed model of two zero-range potentials to an arbitrary number N is quite straightforward without any technical difficulties. The numerical effort increases roughly like N^2. This would yield a model of a cluster in close analogy to the one recently discussed in Ref. [42], but being able to deal with three-dimensional clusters.

There are some limitations of the two-center zero-range potential model, which one has to be aware of: two zero-range potentials, no matter how closely spaced, never overlap. Hence, such a model cannot incorporate internal over-the-barrier ionization, which is responsible for ionization enhancement and subsequent Coulomb explosion within a well-defined range of internuclear separations [43]. Nor does it allow for population trapping since the $1s\sigma_g$ energy surface is not bonding. In a similar vein, the model would yield identical spectra for harmonic generation in H_2^+ and D_2^+ for fixed internuclear separation R. Of course, different distributions of R tailored to mimic vibrational modes in H_2^+ and D_2^+ could be put in by hand. Experimentally, photoelectron spectra of H_2 and D_2 have been found to be largely identical while dissociation of H_2^+ and D_2^+ shows marked isotopy effects [44]. Deficiencies such as these, however, should not affect the calculation of harmonic generation *for a fixed internuclear separation* R. If we intend to model harmonic generation by a particular molecular ion as a function of R then we may as we did in case of H_2^+ readjust the parameters of the two-center zero-range potential for every value of R so as to reproduce the energy surface calculated by other means.

ACKNOWLEDGMENTS

We enjoyed and benefited from discussions with M. Dörr, C. Figueira de Morisson Faria, H. Rottke, and W. Sandner. This work was supported in part by Deutsche Forschungsgemeinschaft.

APPENDIX: GAUGE CONSIDERATIONS

The question of gauge in analytical approximations to multiphoton processes is known to be tricky. If we redevelop the same formalism as above in the length gauge we again end up with the matrix element (25), just the radiation-gauge time-evolution operator $U^{(V_R)}(t,t')$ is replaced by the corresponding time-evolution operator $U^{(V_E)}(t,t')$ in the length gauge. For one zero-range atom at the origin, it is evident that the two gauges yield identical matrix elements. In general, however, this is not so.

Let us consider the matrix element (25) in either gauge $(i=R,L)$,

$$M_{\mathbf{a}}(\boldsymbol{\epsilon},\Omega)=-\frac{e\boldsymbol{\epsilon}^*\cdot}{\hbar^2}\sqrt{\frac{2\pi\Omega}{\hbar V}}\int dt e^{i\Omega t}\int d^3r'd^3r''\times\int_t^\infty dt'\int_{-\infty}^t dt''\phi^*_{0,\mathbf{a}}(\mathbf{r}',t')V_{\mathbf{a}}(\mathbf{r}')\times U^{(V_i)}(\mathbf{r}',t';\mathbf{r}'',t'')\mathbf{r}_{\rm class}(t;\mathbf{r}',t';\mathbf{r}'',t'')\times V_{\mathbf{a}}(\mathbf{r}'')\phi_{0,\mathbf{a}}(\mathbf{r}'',t'') \tag{A1}$$

for a zero-range potential situated at position $\mathbf{a}$ so that

$$V_{\mathbf{a}}(\mathbf{r})=V(\mathbf{r}-\mathbf{a})\quad\text{and}\quad\phi_{0,\mathbf{a}}(\mathbf{r},t)=\phi_0(\mathbf{r}-\mathbf{a},t). \tag{A2}$$

If we shift the integration variables this turns into

$$M(\boldsymbol{\epsilon},\Omega)_{\mathbf{a}}=-\frac{e\boldsymbol{\epsilon}^*\cdot}{\hbar^2}\sqrt{\frac{2\pi\Omega}{\hbar V}}\int dt e^{i\Omega t}\int d^3r'd^3r''\times\int_t^\infty dt'\int_{-\infty}^t dt''\phi^*_0(\mathbf{r}',t')V(\mathbf{r}')\times U^{(V_i)}(\mathbf{r}'+\mathbf{a},t';\mathbf{r}''+\mathbf{a},t'')\times\mathbf{r}_{\rm class}(t;\mathbf{r}'+\mathbf{a},t';\mathbf{r}''+\mathbf{a},t'')V(\mathbf{r}'')\phi_0(\mathbf{r}'',t''). \tag{A3}$$

The classical trajectory $\mathbf{r}_{\rm class}$ does not depend on the gauge. It is just displaced according to

$$r_{\rm class}(t;\mathbf{r}'+\mathbf{a},t';\mathbf{r}''+\mathbf{a},t'')=r_{\rm class}(t;\mathbf{r}',t';\mathbf{r}'',t'')+\mathbf{a}. \tag{A4}$$

The time-evolution operator is translationally invariant in the velocity gauge while in the length gauge it satisfies

$$U^{(V_E)}(\mathbf{r}'+\mathbf{a},t';\mathbf{r}''+\mathbf{a},t'')=e^{-ie\mathbf{a}\cdot[\mathbf{A}(t')-\mathbf{A}(t'')]}U^{(V_E)}(\mathbf{r}',t';\mathbf{r}'',t''). \tag{A5}$$

As a consequence, in the velocity gauge we have

$$M(\boldsymbol{\epsilon},\Omega)_{\mathbf{a}}=M(\boldsymbol{\epsilon},\Omega)_0+\mathbf{a}N(t), \tag{A6}$$

with

$$N(t)=-\frac{e\boldsymbol{\epsilon}^*}{\hbar^2}\sqrt{\frac{2\pi\Omega}{\hbar V}}\int dt e^{i\Omega t}\int d^3r'd^3r''\times\int_t^\infty dt'\int_{-\infty}^t dt''\phi^*_0(\mathbf{r}',t')V(\mathbf{r}')\times U^{(V_R)}(\mathbf{r}',t';\mathbf{r}'',t'')V(\mathbf{r}'')\phi_0(\mathbf{r}'',t''). \tag{A7}$$

The fact that $N(t)$ is time dependent is due to the approximations we have introduced. An exact calculation would yield a constant in place of $N(t)$, and the harmonic spectrum would be translationally invariant as it should. The quantity $N(t)$ has, however, only even harmonic components as can be readily inferred from the explicit form of the time-evolution operator $U^{(V_R)}$, as given, e.g., in Ref. [20]. Hence, in our approximation, the odd harmonic components are not

dependent on the position of the atom. The even components of $N(t)$ generate spurious even harmonics in the spectrum which must not be taken seriously. In the length gauge, on the other hand, the time-evolution operator transforms according to Eq. (A5). The exponential in this equation introduces both even and odd harmonics. As a consequence, shifting the position of the atom mixes even and odd harmonics, and translation invariance holds for neither.

[1] A. L'Huillier, L.-A. Lompré, G. Mainfray, and C. Manus, in *Atoms in Intense Fields*, edited by M. Gavrila, Adv. At. Mol. Opt. Phys. Suppl. **1**, 247 (1992).

[2] P. Salières, A. L'Huillier, Ph. Antoine, and M. Lewenstein, Adv. At. Mol. Opt. Phys. **40B** (1988), edited by B. Bederson and H. Walther.

[3] Z. Chang, A. Rundquist, H. Wang, M. M. Murnane, and H. C. Kapteyn, Phys. Rev. Lett. **79**, 2967 (1997).

[4] Ch. Spielmann, N. H. Burnett, S. Sartania, R. Koppitsch, M. Schnürer, C. Kan, M. Lenzner, P. Wobrauschek, and F. Krausz, Nature (London) **278**, 661 (1997).

[5] M. V. Fedorov, O. V. Kudrevatova, V. P. Makarov, and A. A. Samokhin, Opt. Commun. **13**, 299 (1975).

[6] V. P. Makarov and M. V. Fedorov, Zh. Éksp. Teor. Fiz. **70**, 1185 (1976) [Sov. Phys. JETP **43**, 615 (1976)]; M. V. Fedorov, *ibid.* **73**, 134 (1977) [**46**, 69 (1977)].

[7] A. D. Bandrauk and M. L. Sink, J. Chem. Phys. **74**, 1110 (1981); C. Cornaggia, D. Normand, J. Morellec, G. Mainfray, and C. Manus, Phys. Rev. A **34**, 207 (1986); J. W. J. Verschuur, L. D. Noordam, and H. B. van Linden van den Heuvell, Phys. Rev. A **40**, 4383 (1989); A. Giusti-Suzor, X. He, O. Atabek, and F. H. Mies, Phys. Rev. Lett. **64**, 515 (1990).

[8] P. H. Bucksbaum, A. Zavriyev, H. G. Muller, and D. W. Schumacher, Phys. Rev. Lett. **64**, 1883 (1990); A. Zavriyev, P. H. Bucksbaum, H. G. Muller, and D. W. Schumacher, Phys. Rev. A **42**, 5500 (1990).

[9] A. Giusti-Suzor, F. H. Mies, L. F. DiMauro, E. Charron, and B. Yang, J. Phys. B **28**, 309 (1995).

[10] Y. Liang, S. Augst, S. L. Chin, Y. Beaudoin, and M. Chaker, J. Phys. B **27**, 5119 (1994); D. J. Fraser, M. H. R. Hutchinson, J. P. Marangos, Y. L. Shao, J. W. G. Tisch, and M. Castillejo, *ibid.* **28**, L739 (1995); H. Sakai and K. Miyazaki, Appl. Phys. B: Lasers Opt. **61**, 493 (1995); C. Lyngå, A. L'Huillier, and C.-G. Wahlström, J. Phys. B **29**, 3293 (1996); Y. Liang, A. Talebpour, C. Y. Chien, S. Augst, and S. L. Chin, *ibid.* **30**, 1369 (1997); S. Evans and L. D. Van Woerkom (unpublished).

[11] T. D. Donnelly, T. Ditmire, K. Neuman, M. D. Perry, and R. W. Falcone, Phys. Rev. Lett. **76**, 2472 (1996); J. W. G. Tisch, T. Ditmire, D. J. Fraser, N. Hay, M. B. Mason, E. Springate, J. P. Marangos, and M. H. R. Hutchinson, J. Phys. B **30**, L709 (1997).

[12] M. Yu. Ivanov and P. B. Corkum, Phys. Rev. A **48**, 580 (1993).

[13] T. Zuo, S. Chelkowski, and A. D. Bandrauk, Phys. Rev. A **48**, 3837 (1993).

[14] R. S. Mulliken, J. Chem. Phys. **7**, 20 (1939).

[15] B. Sundaram and P. Milonni, Phys. Rev. A **41**, 6571 (1990).

[16] S. Chelkowski, A. Conjusteau, T. Zuo, and A. D. Bandrauk, Phys. Rev. A **54**, 3235 (1996); S. Chelkowski, C. Foisy, and A. D. Bandrauk, Phys. Rev. A **57**, 1176 (1998).

[17] P. B. Corkum, Phys. Rev. Lett. **71**, 1994 (1993).

[18] K. C. Kulander, K. J. Schafer, and J. L. Krause, in *Super-Intense Laser-Atom Physics*, Vol. 316 of *NATO Advanced Study Institute, Series B: Physics*, edited by B. Piraux *et al.* (Plenum, New York, 1993), p. 95.

[19] M. Lewenstein, Ph. Balcou, M. Yu. Ivanov, A. L'Huillier, and P. B. Corkum, Phys. Rev. A **49**, 2117 (1994).

[20] W. Becker, S. Long, and J. K. McIver, Phys. Rev. A **50**, 1540 (1994).

[21] W. Becker, A. Lohr, M. Kleber, and M. Lewenstein, Phys. Rev. A **56**, 645 (1997).

[22] P. S. Krstić, D. B. Milošević, and R. K. Janev, Phys. Rev. A **44**, 3089 (1991).

[23] Yu. N. Demkov and V. N. Ostrovskii, *Zero-Range Potentials and their Applications in Atomic Physics* (Plenum, New York, 1988).

[24] B. H. Bransden and C. J. Joachain, *Physics of Atoms and Molecules* (Addison-Wesley, Longman Ltd., Essex, 1983).

[25] T. E. Sharp, At. Data **2**, 119 (1971).

[26] W. Becker, A. Lohr, and M. Kleber, Quantum Semiclassic. Opt. **7**, 423 (1995).

[27] P. N. Butcher and D. Cotter, *The Elements of Nonlinear Optics* (Cambridge University Press, Cambridge, 1990).

[28] P. Moreno, L. Plaja, and L. Roso, Phys. Rev. A **55**, R1593 (1997); Laser Phys. **7**, 602 (1997); A. D. Bandrauk, S. Chelkowski, H. Yu, and E. Constant, Phys. Rev. A **56**, R2537 (1997).

[29] B. Gottlieb, A. Lohr, W. Becker, and M. Kleber, Phys. Rev. A **54**, R1022 (1996).

[30] R. Kopold, Diploma thesis, Munich Technical University, 1997.

[31] L. Plaja and L. Roso-Franco, J. Opt. Soc. Am. B **9**, 2210 (1992); A. E. Kaplan and P. Shkolnikov, Phys. Rev. A **49**, 1275 (1994); R. Burlon, G. Ferrante, C. Leone, P. A. Oleinikov, and V. T. Platonenko, J. Opt. Soc. Am. B **13**, 162 (1996); F. I. Gauthey, B. M. Garraway, and P. L. Knight, Phys. Rev. A **56**, 3093 (1997).

[32] S. C. Rae, K. Burnett, and J. Cooper, Phys. Rev. A **50**, 3438 (1994); Ph. Antoine, B. Piraux, D. B. Milošević, and M. Gajda, *ibid.* **54**, R1761 (1996).

[33] C. Figueira de Morisson Faria, M. Dörr, and W. Sandner, Phys. Rev. A **55**, 3961 (1997).

[34] P. Salières, A. L'Huillier, and M. Lewenstein, Phys. Rev. Lett. **74**, 3776 (1995).

[35] Ph. Antoine, M. Gaarde, P. Salières, B. Carré, A. L'Huillier, and M. Lewenstein, in *Multiphoton Processes 1996*, edited by P. Lambropoulos and H. Walther (IOP Publishing, Bristol, 1997), p. 142.

[36] W. Becker, A. Lohr, S. Long, J. K. McIver, B. Chichkov, and B. Wellegehausen, Laser Phys. **7**, 88 (1997).

[37] D. Normand, L. A. Lompré, and C. Cornaggia, J. Phys. B **25**, L497 (1992).

[38] P. Dietrich, D. T. Strickland, M. Laberge, and P. B. Corkum, Phys. Rev. A **47**, 2305 (1993).
[39] J. F. McCann and A. D. Bandrauk, J. Chem. Phys. **96**, 903 (1991); B. Friedrich and D. Herschbach, Phys. Rev. Lett. **74**, 4623 (1995).
[40] R. Numico, A. Keller, and O. Atabek, Phys. Rev. A **52**, 1298 (1995).
[41] H. Stapelfeldt, H. Sakai, E. Constant, and P. B. Corkum, Phys. Rev. A **55**, R3319 (1997).
[42] S. X. Hu and Z. Z. Xu, Phys. Rev. A **56**, 3916 (1997).
[43] T. Seideman, M. Yu. Ivanov, and P. B. Corkum, Phys. Rev. Lett. **75**, 2819 (1995); J. H. Posthumus, K. Codling, L. J. Frasinski, and M. R. Thompson, Laser Phys. **7**, 813 (1997); M. Plummer and J. F. McCann, J. Phys. B **29**, 4625 (1996); **30**, L401 (1997).
[44] H. Rottke, J. Ludwig, and W. Sandner, Phys. Rev. A **54**, 2224 (1996); J. Ludwig, H. Rottke, and W. Sandner, *ibid.* **56**, 2168 (1997).